ADVANCED MATERIALS TECHNOLOGIES
www.advmattechnol.de

3D Printable Polyelectrolyte Complex-Integrated Interpenetrating Network Hydrogels with Customizable Mechanical Strength and pH-Responsiveness

*Vaishali Pruthi, Valerian Hirschberg, and Patrick Théato**

Herein, a novel 3D printable ink designed for the fabrication of interpenetrating polymer network (IPN) hydrogels is introduced, ingeniously integrating a polyelectrolyte complex (PEC) of hyaluronic acid (HA) and chitosan (CS) with a photo-crosslinkable P(OEGMA-*co*-EGDEMA) polymer. Initially, the carboxyl group of HA is modified with a photo-labile *ortho*-nitrobenzyl group, preventing premature PEC formation during 3D ink formulation. Subsequent UV illumination via digital light processing (DLP) simultaneously triggers the photo-deprotection of the carboxyl group of HA and the photopolymerization of OEGMA crosslinked hydrogel, together creating a PEC-integrated IPN hydrogel. Comprehensive characterizations, including NMR, IR, UV/Vis, TGA, DSC, SEM, and mechanical tests are conducted to evaluate the structural, morphological, and rheological properties of these hydrogels. Furthermore, adjustments to the composition of the 3D ink enable the production of hydrogels with a spectrum of mechanical strength and elastic modulus ranging from 1 to 10 kPa. The resultant PEC-IPN hydrogels display excellent flexibility, compressive strength, high strain tolerance, pH responsiveness, and thermal stability. In essence, the approach seamlessly merges natural polyelectrolytes with technological innovation to refine 3D ink production. This method could mark a pivotal advancement in the realm of 3D materials, unlocking numerous prospective applications.

1. Introduction

Hydrogels, distinguished by their hydrophilic nature and 3D cross-linked polymeric structures swollen in water, have become incredibly versatile across numerous areas. For example, they are instrumental in drug delivery[1–3] and tissue engineering,[4,5] as well as in the creation of smart actuators,[6–8] flexible electronic devices,[9] sensors,[10] functional coatings,[11] and water harvesting systems.[12] This versatility stems from their unique characteristics – softness with an ability to tune their mechanical properties, responsive behavior, biocompatibility, bioactivity, unique viscoelastic character, wetness and aptitude for mass transport.[13] On account of these inherent properties, hydrogels have been widely adopted and continue to offer significant benefits for 3D printing applications across various fields.[14,15]

3D printing smart hydrogels is a pathway for developing functional material-based devices.[16] In the past decade, there has been the introduction of various 3D printing techniques like-extrusion-based printing,[16–18] stereolithography (SLA),[19,20] digital light processing (DLP),[21,22] bioprinting,[23] and inkjet printing[13,24] for the fabrication of hydrogel materials.

Among them, DLP stands out due to its unique advantages in precision, speed, and versatility. Digital light processing (DLP) employs a digital light projector to cure photopolymer resins layer by layer, allowing for the creation of intricate structures with high resolution.[21] 3D printing has been extensively used for the production of hydrogels for tissue engineering,[25] drug-loading,[26] scaffolds,[27] regenerative medicines[28] and microfluidic devices.[29] Particularly, the customization of the 3D ink can enhance various desirable properties of the printed structure. A study conducted by Zolfagharian et al. in 2018 reveals the advantage of using a 3D printer to fabricate a chitosan-based polyelectrolyte actuator, comparing its performance with conventional cast chitosan.[30] By employing naturally occurring, biocompatible, and biodegradable polymer materials, it is possible to create intricate and responsive hydrogel structures through additive manufacturing.

Among the wide array of bioinks currently being investigated, hyaluronic acid (HA) and its derivatives hold a distinct position. Hyaluronan, a constituent of the extracellular matrix, is a glycosaminoglycan characterized by its high molecular weight. It

V. Pruthi, V. Hirschberg, P. Théato
Institute for Chemical Technology and Polymer Chemistry (ITCP)
Karlsruhe Institute of Technology
Kaiserstraße 12, 76131 Karlsruhe, Germany
E-mail: patrick.theato@kit.edu
P. Théato
Soft Matter Synthesis Laboratory
Institute for Biological Interfaces III
Hermann-von-Helmholtz-Platz 1, Eggenstein-Leopoldshafen, 76344 Karlsruhe, Germany

The ORCID identification number(s) for the author(s) of this article can be found under https://doi.org/10.1002/admt.202400416

DOI: 10.1002/admt.202400416

is uniquely structured, comprising repetitive disaccharide units, specifically *N*-acetylglucosamine and glucuronic acid. HA's biological relevance and cytocompatibility are key features, complemented by its shear-thinning properties. Additionally, its unique viscoelastic nature and capacity for precise fine-tuning of desired attributes through chemical modifications further underscore its significant potential in the field.[31]

Acting as a biocompatible polycationic natural polymer, chitosan can also be crosslinked with HA to form a polyelectrolyte complex (PEC).[32] Chitosan, a natural, mildly polycationic compound, consists of non-linearly structured units of *N*-acetylglucosamine and glucosamine. Owing to its desirable physicochemical characteristics, optimal viscosity, and cell adhesion capabilities, it is deemed fit for bioprinting applications.[23,33] PECs are physically crosslinked as a result of electrostatic interaction between two oppositely charged polyelectrolytes and the entropic-driven release of small counter ions.[34] In comparison to covalently crosslinked hydrogels, PEC exhibits greater sensitivity to swelling, particularly in response to pH variations.[32] But when exposed to aqueous environments, PEC undergoes continuous swelling and will ultimately dissolve, which results in the breakdown of their structural integrity. However, by achieving controlled and adjustable swelling, it is possible to prevent the loss of material, maintain the stability of the structure and mechanical characteristics, and preserve the functionalities of PEC hydrogels.[35] They offer a promising foundation for creating soft materials tailored for various biomedical applications. These applications range from serving as scaffolds in tissue engineering,[25,36] drug delivery,[37,38] ionic conductors[39,40] and food industry.[41,42] The mechanical robustness of PEC hydrogels can also be modulated by varying the reactive ion pairs. In 2018, Liu et al. reported the fabrication of a 3D-printed PEC hydrogel by polycomplexation of alginate and chitosan.[25]

Among the extensive range of polymeric-based matrices, interpenetrating networks (IPNs) and semi-IPNs membranes stand out due to their exceptional adjustability in composition and physicochemical properties. This adaptability is facilitated by integrating various polymers and utilizing different crosslinking techniques. These innovative systems exhibit impressive enhancements in both stability and mechanical strength, primarily attributable to molecular reinforcement due to the interwoven networks of diverse polymers.[43] IPN is a structure formed by two or more polymer networks that are interlinked, either physically or chemically, and intertwined with one another. On the other hand, a semi-IPN is slightly different, with only one polymer undergoing crosslinking.[44,45] In 2016, Bootsma et al. fabricated complex and tunable IPN hydrogel materials possessing tissue mimetic properties using dual syringe 3D printing technique.[46]

Moreover, a recent study by Li et al. reported the creation of PEC-IPN hydrogels in order to overcome the drawback of PEC by interlacing it in a covalent network.[47] They highlighted the synergic improvements in the mechanical properties of the hydrogel network by incorporating PEC in IPN. Although 3D printing of PEC and IPN has been studied separately, research on 3D printing of such PEC containing IPN hydrogels is still emergent, which motivated us for the present study. The quest to efficiently 3D print IPN hydrogels faces intriguing challenges, especially in understanding and manipulating their viscoelastic properties. This research gap is critical, as these properties are pivotal in material applications.

Herein, we designed a unique approach for 3D printing of IPN hydrogels, containing PEC of HA/CS and photo-crosslinkable P(OEGMA-*co*-EGDEMA) polymer. First, we synthesized an *ortho*-nitrobenzyl protected ester of hyaluronic acid in order to avoid the PEC formation while mixing the polyelectrolytes (PEs) in the 3D ink. The strategy is to induce the photodeprotection of the carboxyl group of HA and the photopolymerization of OEGMA crosslinked hydrogel simultaneously under UV using digital light processing (DLP). Moreover, we fabricated and optimized the photopolymer, semi-IPNs and IPNs using conventional methods for 3D printing. All the synthesized hydrogels were characterized by studying their structural, morphological and rheological properties. The composition of the 3D ink was adjusted and modified for further improvement, enabling the production of hydrogels with diverse mechanical strengths. The comparative pH-induced swelling properties of the hydrogels were also investigated in this work. Therefore, we report a technique to print PEC-containing IPN hydrogels with variable mechanical properties. This strategy could herald a major leap forward in the field of 3D materials, paving the way for numerous emerging applications.

2. Results and Discussion

2.1. Composition of 3D Ink

For the fabrication of PEC-containing IPN hydrogels, the initial step was to prepare the photo resin (3D ink) and optimize its composition. The strategy is to enable simultaneous photodeprotection and photo-polymerization in the photoresin when exposed to UV light. **Figure 1** illustrates the method employed for the formulation of 3D ink. To do so, naturally available, oppositely charged biopolymers—chitosan (CS) (a cationic polyelectrolyte) and hyaluronic acid (HA) (an anionic polyelectrolyte), were employed. Firstly, in order to avoid the PEC formation before printing, the carboxyl groups of hyaluronic acid were protected using an *ortho*-nitrobenzyl photo-labile protecting group (PPG). On exposure to UV light at 365 nm, the PPG is cleaved due to photo-induced deprotection and the COOH functionality is restored, which leads to the formation of PEC.

Further, to induce photopolymerization in the 3D ink, oligo(ethylene glycol) methyl ether methacrylate (OEGMA), ethylene glycol dimethylacrylate (EGDEMA) and lithium phenyl-2,4,6-trimethylbenzoylphosphinate (LAP) were used as a polymerizable vinyl monomer, crosslinker, and water-soluble photoinitiator, respectively. LAP is a suitable candidate for 3D inks to form hydrogels as it offers a balance between biocompatibility as well as photon absorption, along with a high polymerization rate at low concentrations.[48]

2.2. Protection and Deprotection of Hyaluronic Acid Using *Ortho*-Nitrobenzyl PPG

2.2.1. Protection of HA Using Photolabile Group

The photo-labile protection of the carboxyl group on hyaluronic acid was achieved by grafting the *o*-NB groups onto

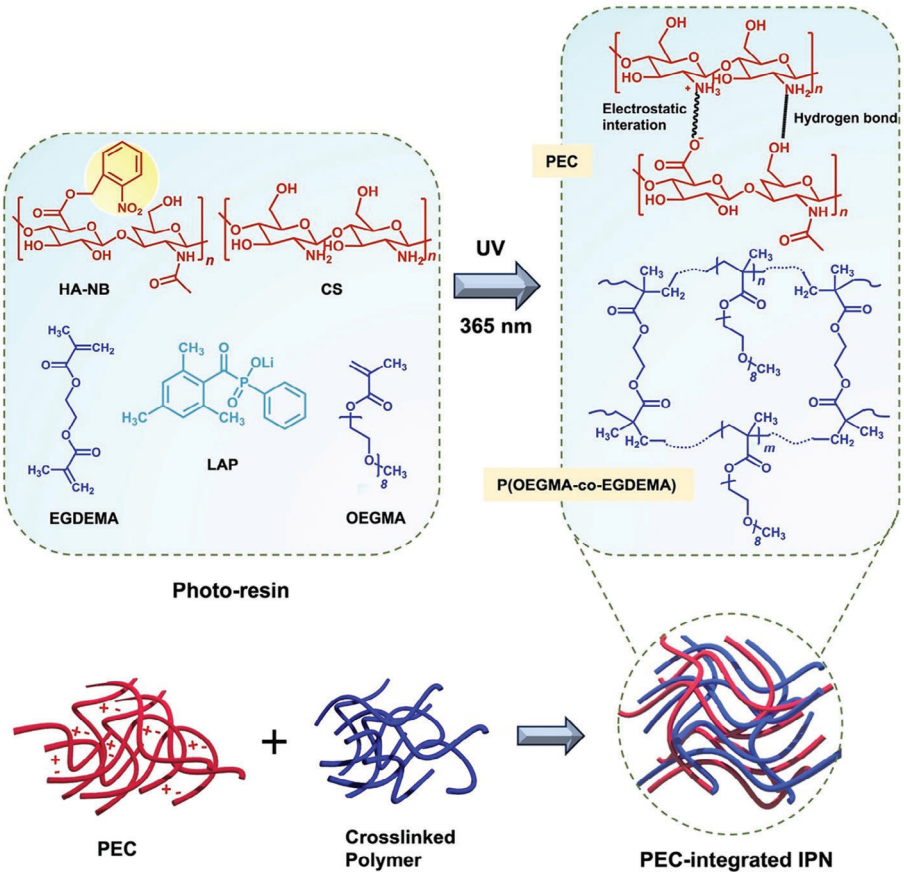

Figure 1. Conceptual diagram detailing the methodology for 3D ink formulation.

carboxylic acid groups of HA chains through an ester linkage (**Scheme** 1a). The HA salt was esterified with *ortho*-nitrobenzyl chloride, resulting in the formation of *o*-NB HA ester. By varying the amount of *ortho*-nitrobenzyl chloride added to the mixture, various *o*-NB grafted HA derivatives were obtained.

The IR spectra of the product confirmed the presence of the *ortho*-nitrobenzyl group (**Figure** 2a). The characteristic bands of the —NO_2 group were observed at 1526 and 1346 cm^{-1}, and the ester peak at 1750 cm^{-1}. The esterification was further validated using the ^{1}H NMR of HA-NB (Figure 2b). ^{1}H NMR of the obtained *ortho*-nitrobenzyl ester of HA showed the characteristic shifts at 7.5 to 8.2 ppm for the aromatic (—C_6H_4—), along with the shifts at 3.1 to 4 ppm. The *o*-NB grafting degree was calculated by integrating the NMR signal from the aromatic protons in the *o*-NB group and the NMR signals from the anomeric protons of the disaccharide units in HA. Moreover, UV/vis spectroscopy was conducted for various HA-NBs with different grafting degrees, dissolved in water at a concentration of 0.2 mg mL^{-1}. The resulting spectra are depicted in Figure 2c.

2.2.2. Photo-Deprotection

The *o*-NB protecting group can be easily cleaved when irradiated with UV light (365 nm), as shown in Scheme 1b. Upon UV exposure, the *o*-NB ester linkage undergoes a photo-induced cleavage upon UV irradiation, resulting in the release of HA and the formation of a nitrosobenzaldehyde byproduct. This could be confirmed by the NMR spectra at different intervals of UV-irradiation on HA-NB as shown in Figure 2d. The new peaks arising at 9.36 and 10.25 ppm, representing the aldehyde CHO group in nitrosobenzaldehyde and the free COOH carboxylic acid group of HA, respectively, confirm the deprotection of HA-NB. The photo-deprotection of the HA-NB derivative was also studied using UV/vis spectroscopy (Figure 2e). A change in the color of the HA-NB solution was noted when exposed to UV ($\lambda \approx 365$ nm) over a period of time, transitioning from a light yellow ($t = 0$ min) to a deeper yellow hue ($t = 360$ min) (Figure 2f). The time taken for photo-cleavage also depended on the intensity of light irradiated and the degree of NB grafting on HA.[49]

2.3. 3D Ink Formulation

In order to establish the optimal composition of the photoresin for 3D printing applications, the initial step involves optimizing the formulation of 3D ink. This process was undertaken by first synthesizing photo-polymers using the standard cast-mold technique, employing a UV lamp with a 365 nm wavelength as the illuminating source. The optimized compositions for the photo-induced syntheses of the hydrogels are detailed in **Table** 1.

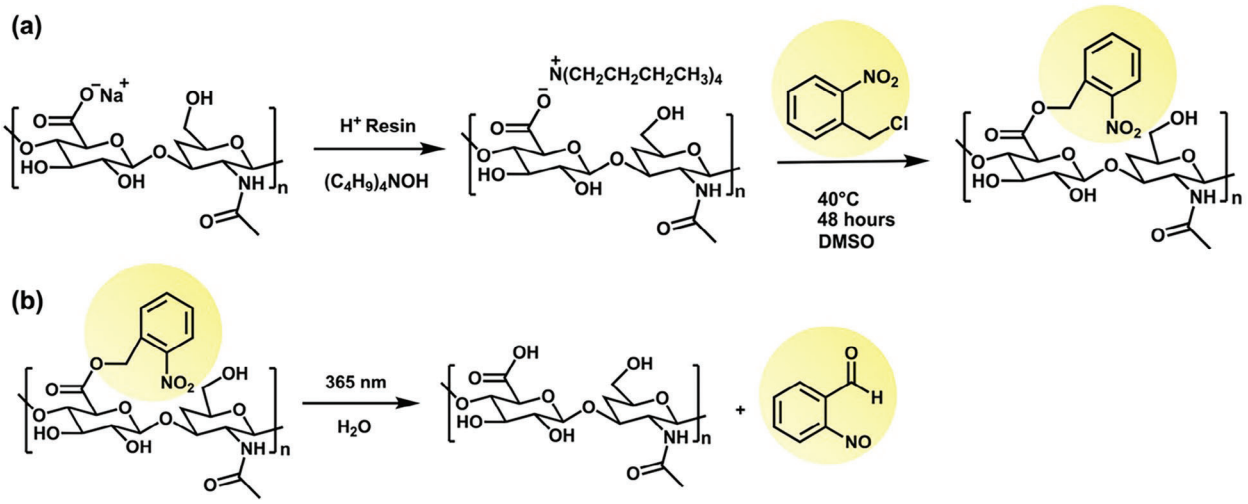

Scheme 1. a) Synthetic route for the protection of HA using *ortho*-nitrobenzyl photo-labile protecting group, b) deprotection of *ortho*-nitrobenzyl ester of HA (HA-NB).

2.3.1. Photocrosslinkable P(OEGMA-co-EGDEMA) Hydrogel

A variety of photopolymers were produced by adjusting the amounts and combinations of three components: OEGMA as the monomer, EGDEMA as a crosslinker, and LAP as the photoinitiator. The mixture was subjected to UV light (365 nm) for the fabrication of hydrogels. The crosslinker ratio was tuned to adjust the crosslinking density, with an excess potentially leading to brittleness. Also, the photoinitiator concentration was regulated to refine the speed and efficiency of curing. An optimal concentration range of 2–4 mol% for EGDEMA and 1 wt% LAP was determined. The completion of crosslinking and photopolymerization was confirmed through the use of infrared (IR) spectroscopy. As depicted in the IR spectra (**Figure 3a**), the C═C bonds in the methacrylate group (1637 cm^{-1}) of OEGMA and EGDEMA disappeared after photopolymerization and symmetric methylene stretching (—CH_2) at 2870 cm^{-1} remained as it does not participate in the polymerization.

2.3.2. PEC Hydrogel of HA-NB and CS

PEC hydrogels were prepared by mixing different proportions of HA-NB and CS to optimize the ratio that would result in a stable hydrogel film. The hydrogel comprising HA-NB/ CS with the ratio of 1:1 was found to be the most stable, probably as a result of maximum complexation due to the strongest ionic interaction. As shown in Figure 3b, the IR spectra of dried PEC film was compared with that of HA-NB and CS. The IR spectra of PEC showed bands between 1560 cm^{-1} and 1650 cm^{-1} representing C═O, N—H and C—N vibrations. It confirms the ionic interaction between carboxylic acid group of HA and amine group of CS, hence the formation of PEC. Moreover, a slight shift in the position and changes in the intensity and shape of the O—H (3200 to 3600 cm^{-1}) and N—H (≈3200 to 3600 cm^{-1}) bands in PEC spectra also could be seen as a result of hydrogen bonding between HA and CS.

2.3.3. Semi-IPN Hydrogel Containing Hyaluronic Acid or Chitosan

The formation of semi-IPNs comprised of either HA or CS involved dissolving them separately with a trio of OEGMA, EGDEMA, and LAP, and using UV light to induce gelation. The concentration of polyelectrolyte was varied in order to optimize the dissolution of the mixture and the stability of the hydrogel. Figure 3c displays the IR spectra of semi-IPN containing HA, highlighting the distinctive bands of both HA and

Table 1. Optimized composition for the photo-induced synthesis of hydrogels.

Photopoymerized hydrogel	OEGMA [g]	EGDEMA [mol%]	LAP [wt%]	HA [mg]	HA-NB [mg]	CS [mg]	Gelling time[a] [min]	Elastic modulus[b] [kPa]
P(OEGMA- *co* -EGDEMA)	0.5	3	1	–	–	–	5	1
Semi-IPN with CS	0.5	3	1	–	–	2.5	5	4
Semi-IPN with HA	0.5	3	1	2.5	–	–	5	2
IPN (HA-$NB_{0.5}$/CS) 1:1	0.5	3	1	–	2.5	2.5	15	8
IPN (HA-$NB_{0.5}$/CS) 1:2	0.5	3	1	–	5.0	2.5	15	6.5
IPN (HA-$NB_{0.5}$/CS)2:1	0.5	3	1	–	2.5	5.0	15	7

[a] Gelling time was calculated by measuring the time it takes for a liquid precursor to form a gel); [b] Elastic modulus was determined through rheological assessments.

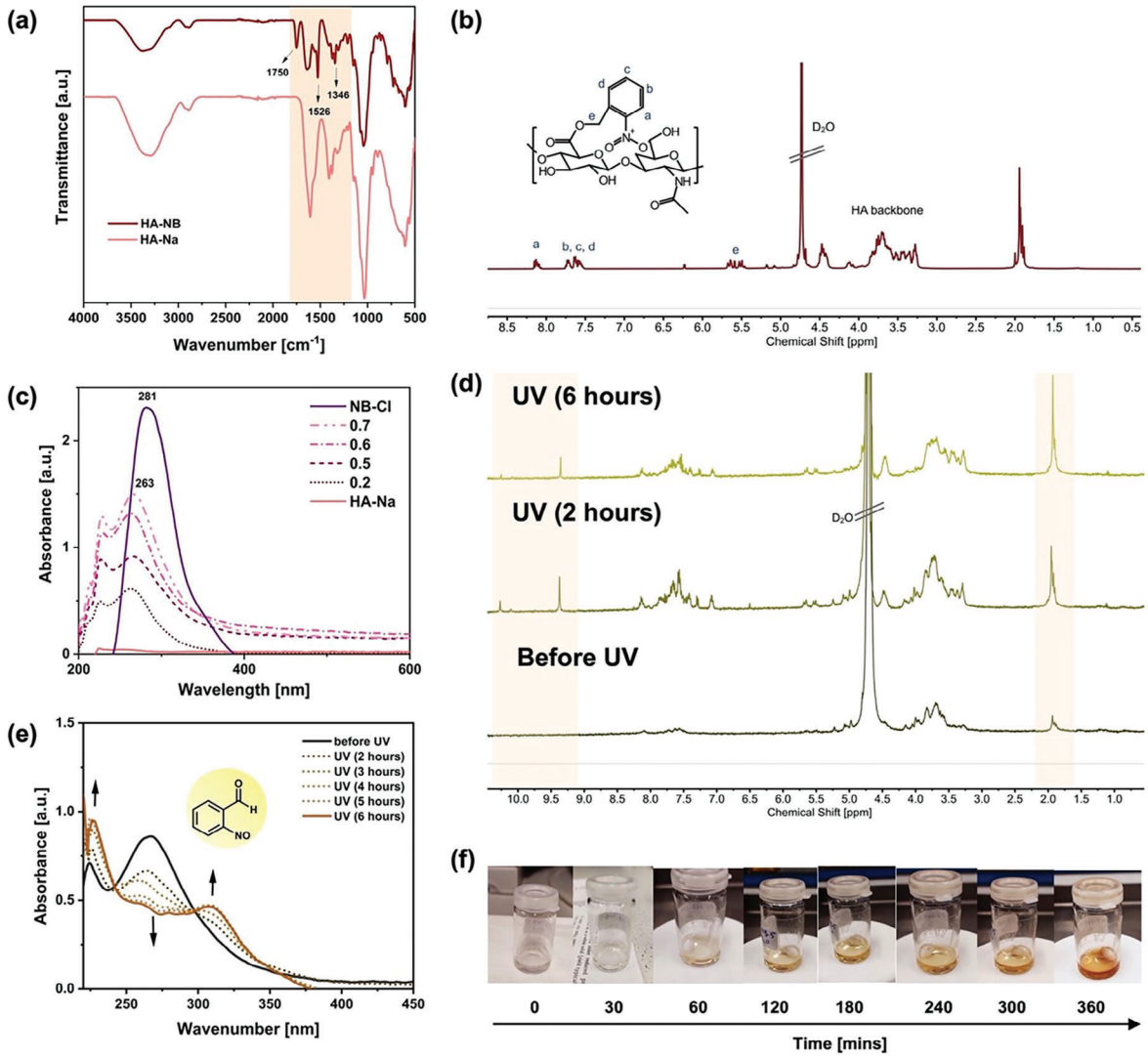

Figure 2. a) IR spectra comparing HA-Na and HA-NB, b) ^{1}H NMR spectra of HA-NB in D_2O, c) UV/Vis absorption spectra of HA-NBs highlighting variations in grafting degrees, d) ^{1}H NMR spectra (400 MHz, 298 K) presenting the deprotection process of HA-NB in D_2O at distinct photo-irradiation time points, e) UV/Vis absorption profiles demonstrating the deprotection of HA-NB upon UV exposure at various intervals (note: all spectra were acquired in D_2O at a concentration of 0.2 mg mL^{-1}) and f) time-dependent color transition in HA-NB solution under UV light exposure.

P(OEGMA-*co*-EGDEMA). Similarly, it presents the IR spectra for the semi-IPN with CS, emphasizing the characteristic bands of CS and P(OEGMA-*co*-EGDEMA).

2.3.4. Polyelectrolyte Complex (PEC) Containing IPN Hydrogel

PEC-incorporated IPN hydrogels with varying properties were fabricated by using HA-NBs with different grafting degrees (0.2 to 0.7) and by adjusting the ratio of the HA-NB and CS components (i.e., 1:1, 1:2, 2:1) in the blend, containing OEGMA, EGDEMA and LAP. The proportions of polyelectrolytes were varied to investigate their effect on the degree of ionic interaction and complexation within the hydrogel. The simultaneous photo-polymerization and photo-cleavage of *o*-NB ester linkage was achieved by exposure to UV light (365 nm). The IR spectrum of IPN with PEC (HA-NB/CS) is shown in Figure 3c, which also displays the band at 1640 cm^{-1}, confirming the ionic interaction between HA and CS. Figure 3d,e displays the IPN hydrogels produced using the invert-vial method, while Figure 3f showcases the lyophilized hydrogel.

2.3.5. Optimized 3D Hydrogel Ink Formulation

To achieve the desired crosslinking density, mechanical properties, curing efficiency, and printability of the hydrogels, the photoresin's optimized composition was established through the synthesis methods mentioned earlier. It was scaled up in order to prepare sufficient ink (≈10 mL) in the resin tank, to process the printing. For this, a PEC-integrated IPN hydrogel ink was prepared by dissolving the solution of 50 mg HA-NB in water, 10 g

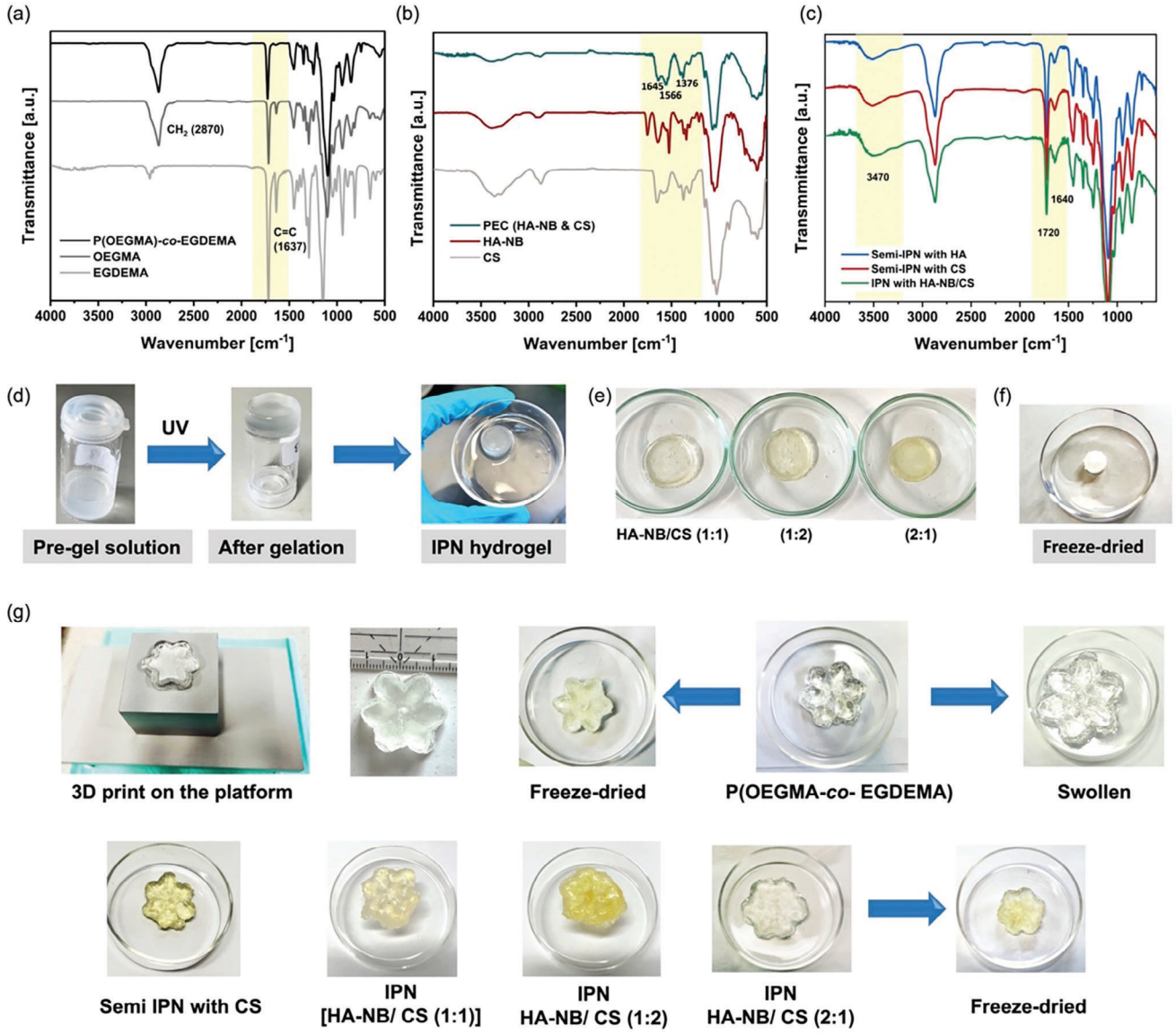

Figure 3. IR spectra of a) P(OEGMA- *co* -EGDEMA) hydrogel alongside its individual components: OEGMA and EGDEMA, b) PEC(HA-NB/ CS) in comparison to HA-NB and CS, c) semi-IPNs and IPN hydrogels, d) visualization of hydrogel formation via the invert-vial technique used for optimization of composition of 3D ink, e) IPNs with different proportions of HA-NB and CS, f) lyophilized (freeze-dried) IPN hydrogel, g) photographic captures of 3D printed hydrogels (printed using Miicraft Hyper 80×3D printer with UV = 365 nm).

OEGMA, 0.079 g EGDEMA (2 mol%) and 0.10 g LAP (1 wt%) solution in 3 mL water. Then, a solution of 50 mg CS in 1% AA was added to the mixture. The mixture was stirred for 15 min to completely dissolve all the components. Once a homogenous mixture was obtained, it was then poured into the resin tank of the DLP 3D printer for printing.

2.4. 3D Printing of Hydrogels

The 3D ink optimized in the previous step was employed for the 3D printing of hydrogels. In order to print the hydrogels, the components of the 3D ink were blended together to prepare a homogenous mixture and this ink was then transferred to the resin bath of a digital light processing (DLP) printer. When optimizing the 3D ink formulation, the interplay between the chemistry of the ink and the DLP printer settings was considered. The photo-resin was tuned to adjust the ink's viscosity (by varying the ratio of constituents) and curing depth (by modifying the photo-initiator composition). Additionally, the printing parameters such as- light intensity (365 nm), base curing exposure time (50 s), layer thickness (20 µm) and printing speed (slow) were adjusted in order to refine the printed material. (More details are mentioned in Table S1 and Figure S6, Supporting Information). PEC-based IPN hydrogels with variable compositions of HA-NB and CS were successfully printed as shown in Figure 3g.

2.5. Properties of Hydrogels

2.5.1. Swelling Properties

Swelling was measured in terms of the percentage increase in weight, indicating the amount of water the hydrogel had absorbed (Equation S1, Supporting Information). The graph representing the comparison in the swelling percentage of all the hydrogels is depicted in **Figure 4a**. The hydrogel pictures in Figure 4b clearly show the remarkable difference in the size of the hydrogels when swollen till equilibrium.

The comparative trend observed in the swelling is as follows: IPN hydrogels > semi-IPN hydrogels > P(OEGMA-*co*-EGDEMA) hydrogel, with the equilibrium swelling percentages as follows: PEC-integrated IPN hydrogels at 2455%, Semi-IPN with HA at 1127%, semi-IPN with CS at 780%, and P(OEGMA-*co*-EGDEMA) hydrogel at 532%. The pronounced swelling ability of the polyelectrolyte IPN gels can be attributed to the electrostatic forces that drive the charged groups on the polymer chains apart.[50] Both HA and CS, being natural polysaccharides, possess hydrophilic characteristics, though they differ slightly in their water retention abilities.

2.5.2. pH-Induced Swelling

The swelling behavior of the synthesized hydrogels was also investigated at different pH values of pH 1, 3, 5, 7 and 11. As depicted in Figure 4c, the IPN hydrogels exhibited maximum swelling at pH = 3 and minimum at pH = 5. At pH = 7, the swelling again increased and was observed to be higher at pH = 11. This could be explained as PEC hydrogels are created through ionic interaction and the extent to which they swell is governed by the pH-responsive charge interactions of the two polymers.[51] Furthermore, they possessed a notable water content and high electric charge, facilitating the diffusion of water.[32] When pH changed, the charge balance as well as the degree of interaction between HA and CS also fluctuated. The lowest swelling occurred when pK_a(anionic)<pH<pK_a(cationic).[52] pK_a of HA and CS are 3 and 6.5, respectively. Therefore, at low pH, amino groups of CS are ionized and at pH > 6.5, carboxyl groups of HA are ionized, resulting in higher swelling. The swelling ratio is least at pH = 5, as a result of strong electrostatic interactions between the polyelectrolytes.

Additionally, swelling was also dependent on the relative proportion of polyelectrolytes in PEC as illustrated in Figure 4c. This is attributed to the change in the degree of interaction and crosslinking density in the PEC.[32] Therefore, it is possible to modulate the properties of PEC-IPN hydrogel by tuning its composition. Hydrogels of this nature, characterized by pH-responsive swelling and adjustable attributes, hold immense potential across a wide array of applications, including drug delivery systems and the field of soft robotics.

2.5.3. Morphological Properties

Figure 4d shows scanning electron microscopy (SEM) images of freeze-dried P(OEGMA-*co*-EGDEMA), semi-IPN with CS, semi-IPN with HA and IPN with HA-NB/CS (1:1) hydrogels. The observed porosity in these hydrogels aligns well with the swelling percentage calculated for each hydrogel. This is due to the fact that the equilibrium water uptake of hydrogels notably rises with an increase in porosity.[53] Moreover, the different components in the semi-IPN and IPN structures had distinct effects on the porosity of the hydrogels. Introducing HA to the hydrogel resulted in a greater increase in porosity compared to adding CS. This could be due to their different interactions with the polymer matrix. Further, the combination of HA and CS in the IPN, containing P(OEGMA-*co*-EGDEMA) resulted in the largest pores, suggesting a potential synergistic effect or complexation between these components. This could be attributed to the entropy and strong electrostatic attraction between the oppositely charged polymers.[54]

2.5.4. Thermal Properties

Thermal characterization of the synthesized hydrogels was performed by employing thermogravimetric analysis (TGA) and differential scanning calorimetry (DSC) techniques to provide a comprehensive understanding of their thermal stability and durability. Figure 4e represents the comparative TGA curves for the freeze-dried hydrogels. All the fabricated hydrogels showed a high thermal decomposition temperature (T_d (5%)) ranging between 220 °C to 290 °C, indicating high thermal stability levels. Such resilience to heat ensures that these hydrogels can be employed across various applications where elevated temperatures are encountered, maintaining their integrity and functional performance without degradation. Furthermore, the DSC graphs of the swollen hydrogel samples are illustrated in Figure 4f. DSC serves as a crucial method for identifying the physical state of water within the hydrophilic polymer.[55] The DSC of all hydrogels showed an endothermic peak at around 1 °C and 10 °C which is probably attributed to the melting of freezing bound water and freezing free water in the hydrogels, respectively. Additionally, the endothermic peak representing the vaporization of non-freezable bound water, varying from 107 °C in semi-IPNs, 110 °C in IPN and 114 °C in P(OEGMA-*co*-EGDEMA) can be observed. This variation could be associated with the changes in the degree of crosslinking, water-polymer interactions and hydrophilicity.[56] The interplay among the charged polymer chains present in HA and CS introduces a subtle shift in the peak and gives rise to an additional shoulder on the DSC curve. Furthermore, the variations in the area under the endothermic peak in various hydrogels can be attributed to the differing complexities of their structures and the varying amounts of water they retain within their matrices. (Figure S5, Supporting Information).

2.5.5. Tunable Mechanical Properties

To analyze the mechanical behavior of the prepared hydrogels and to understand the influence of different components on their mechanical properties, strain and frequency-dependent shear rheology to study the flow behavior and uniaxial compression tests were conducted to measure the storage (G') and loss modulus (G'') at room temperature (20 °C) and an angular frequency ranging from 0.1 to 100 rad s^{-1}.[44,57]

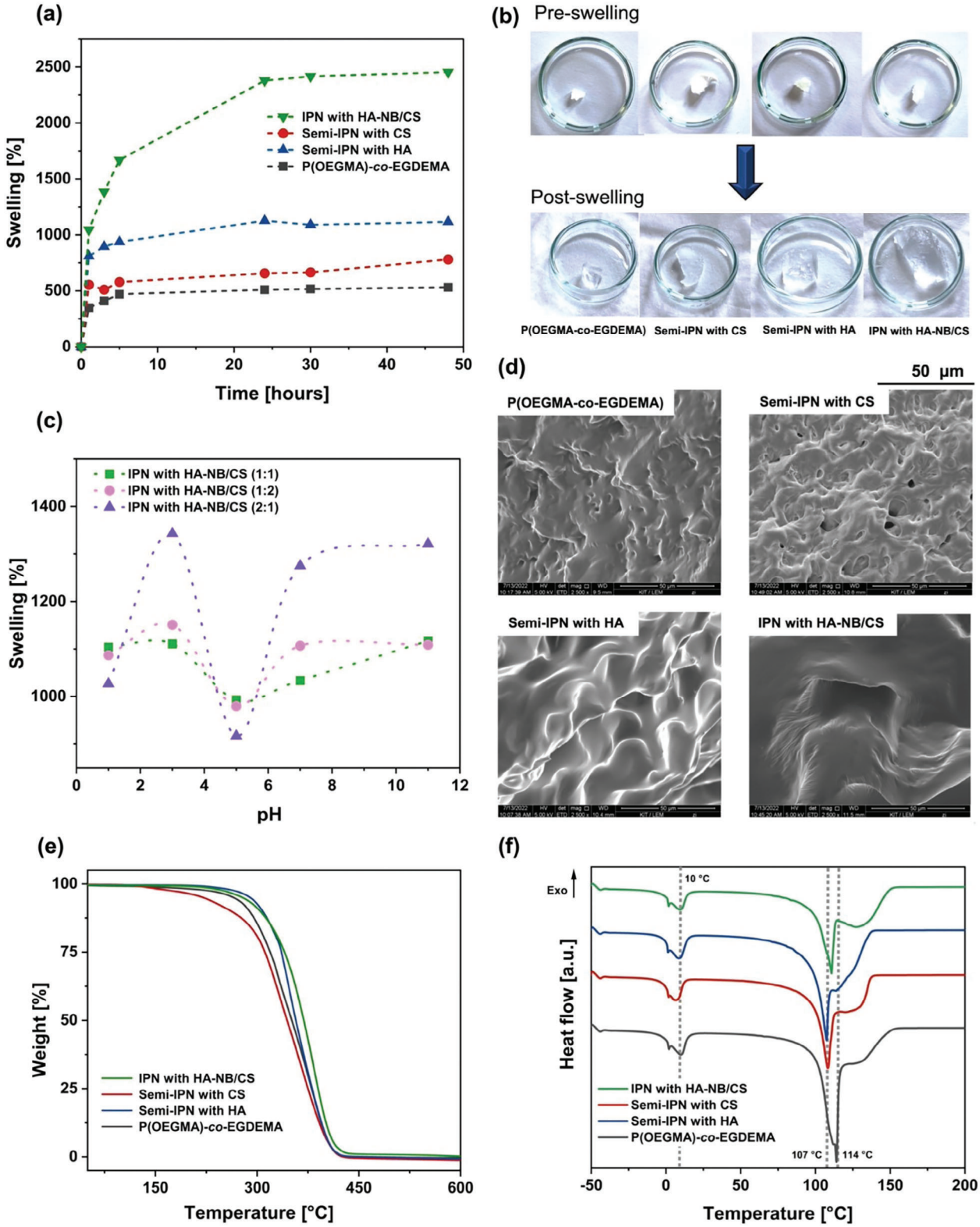

Figure 4. a) Comparative analysis of swelling percentages among various hydrogels, b) representative images of hydrogels pre- and post-swelling, c) pH-responsive swelling behavior of IPN hydrogels with varying polyelectrolyte content, d) SEM micrographs illustrating the differential porosity (Magnification = 2500×), e) TGA profiles and f) DSC plots of P(OEGMA-*co*-EGDEMA), semi-IPNs and IPN hydrogels.

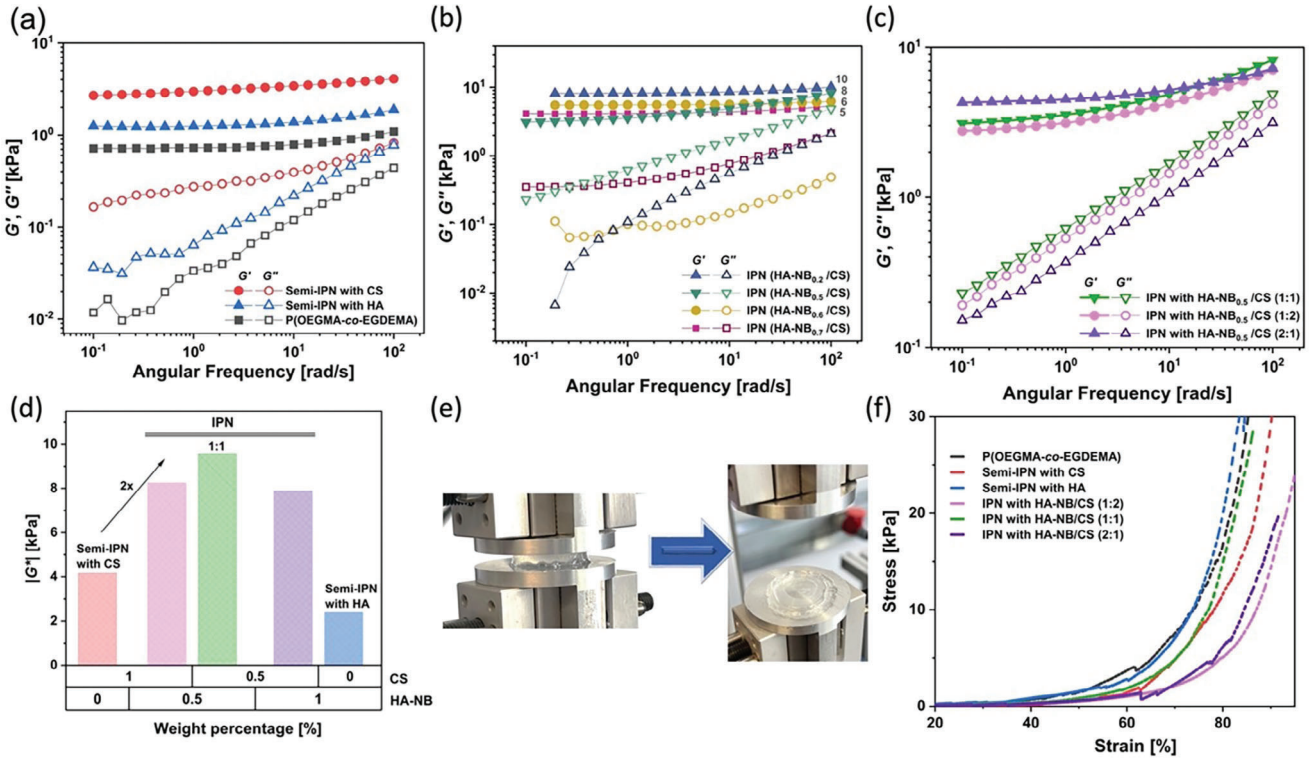

Figure 5. Frequency sweep analyses demonstrating the viscoelastic properties via storage and loss modulus measurements for a) P(OEGMA-*co*-EGDEMA), semi-IPNs, and IPN hydrogels, b) IPNs integrated with HA-NB of varied grafting degrees, c) IPNs containing diverse ratios of polyelectrolytes, d) relationship between complex modulus $|G^*|$ and weight percentage of various polyelectrolytes at an angular frequency of 100 rad s^{-1}, e) depiction of hydrogel resilience, maintaining integrity even under substantial compression at a strain of 80% and f) stress-strain profiles derived from compressive testing of hydrogels.

For all examined hydrogels, rheological analysis consistently reveals a higher value of G' relative to G'', indicating a dominantly elastic ("solid-like") behavior of gels over viscous behavior.[47] This suggests that the hydrogels possess a robust internal polymer network capable of maintaining structural integrity and recovering to its original form/shape upon stress removal.

As illustrated in **Figure** 5a, introducing a polyelectrolyte into the P(OEGMA-*co*-EGDEMA) hydrogel network increased G' and G'', thereby enhancing the hydrogel's stiffness. Furthermore, the semi-IPN with CS integrated into P(OEGMA-*co*-EGDEMA) exhibited a stiffer network ($G' \approx 4$ kPa) compared to the semi-IPN with integrated HA ($G' \approx 2$ kPa). IPNs that incorporated PEC (HA/CS) displayed even higher G' values (ranging from 5 to 10 kPa). This increase is attributed to heightened molecular interactions, complex formation, and higher crosslinking density due to the presence of two crosslinked networks within the IPN hydrogel system.

Consequently, PEC-IPN hydrogels with different mechanical strengths were achieved using HA-NB with varying grafting ratios of the *o*-NB group. Figure 5b illustrates the relationship between the grafting degree of *o*-NB and the changes in the storage modulus (G') and the loss modulus (G''). Notably, as the grafting degree of HA-NB decreased, G' increased. This trend may be attributed to a higher degree of complexation and the formation of a denser network structure in the IPN with the lowest grafting degree of HA-NB, specifically IPN(HA-$NB_{0.2}$/CS) which displayed a G' of 10 kPa at a frequency of 100 rad/s. Such a structure limits the mobility of the polymer chains, thereby enhancing the material's rigidity and leading to a larger G' compared to G''. On the other hand, the IPN(HA-$NB_{0.5}$/CS) demonstrated values of G' and G'' that were closer together, signifying a comparably less elastic material and a higher viscous contribution in the mechanical response.

Figure 5c further illustrates the impact of the ratios of HA-$NB_{0.5}$ and CS on G' and G'' of the PEC-integrated hydrogel. Notably, the IPN with a (HA-$NB_{0.5}$/CS) ratio of 1:1 exhibited a higher G' (8 kPa) and G'' (3 kPa) compared to the 1:2 and 2:1 HA-$NB_{0.5}$:CS ratios at the angular frequency of 100 rad s^{-1}. Therefore, the 1:1 ratio of HA-NB and CS provides an optimal crosslinking density, resulting in a balance between the rigidity provided by crosslinks and the flexibility necessary for some movement within the network.

Figure 5d displays a bar graph that highlights the variations in the complex modulus ($|G^*|$) of the hydrogels based on their different compositions. The integration of HA-NB with CS within an interpenetrating network (IPN) significantly augmented $|G^*|$ relative to semi-IPNs composed exclusively of HA and CS. This could be ascribed to the optimal synergy and strong electrostatic interaction in PEC, resulting in a more structurally cohesive and mechanically robust network.[47] Moreover, the elevated $|G^*|$ values observed in IPNs validate the development of a polymer matrix that possesses reinforced structural integrity and augmented

resistance to deformation. The IPN configuration with a balanced 1:1 HA-NB/CS ratio is distinguished by its superior mechanical resilience, as evidenced by its highest |*G**| value, which is 2x the value for Semi-IPN with CS.

Therefore, we demonstrate that by judiciously altering the network structure and molecular composition, it is feasible to precisely engineer the mechanical properties of hydrogel networks to meet bespoke application requirements. Prior studies, notably in 2021, have showcased printed PEC hydrogels derived from HA and CS with shear storage moduli within the range of 0.1 to 1 kPa.[58] Here, we present a notable enhancement in the mechanical strength of our 3D printable IPN hydrogel, with *G'* values registering between 5 to 10 kPa, attributable to the incorporation of PEC into the crosslinked P(OEGMA-*co*-EGDEMA) framework. This is in agreement with the reported literature that indicates the cumulative effects of network interactions enhancing mechanical performance beyond that of individual components.[47]

Additionally, compression tests were also performed for all the hydrogels for comparative analysis. The IPN hydrogel featured in Figure 5e demonstrated its durability by resisting breakage even under intense compression at a strain of 80%. The stress-strain graph of hydrogels illustrated in Figure 5f reveals that these hydrogels could endure substantial strain without breaking. Therefore, all the fabricated hydrogels demonstrated good mechanical properties, and outstanding compression properties, coupled with high flexibility and stretchability (Figures S3 and S8, Supporting Information).

3. Conclusion

In our study, we introduced the formulation of a novel 3D ink for printing IPN hydrogels by skillfully combining the PEC of HA and CS with a photo-crosslinked network of P(OEGMA-*co*-EGDEMA) polymer. Firstly, we modified the carboxyl group on HA with a photolabile *ortho*-nitrobenzyl group to avoid the early formation of the PEC during 3D ink development. This alteration culminated in a dynamic UV-mediated process, wherein the carboxyl group was photo-deprotected and the OEGMA hydrogel was crosslinked in a simultaneous action. In-depth characterizations of the hydrogels underscored their structural, morphological, and rheological properties. We also evaluated their swelling dynamics as well as their pH sensitivity. After refining the composition of the 3D ink, the fabricated IPN hydrogels created had mechanical attributes with *G'* spanning 5 to 10 kPa, displaying significant flexibility, commendable compression resistance, and high strain tolerance. This level of customization is what sets our work apart from others in the literature, as it provides a versatile platform for creating tailor-made hydrogels with desired characteristics. Thus, our research presents a promising approach for the fabrication and 3D printing of PEC-integrated IPN hydrogels with regulated swelling and the maintenance of structural stability, mechanical robustness, and intrinsic functions within the hydrogels. Their pH sensitivity and excellent thermal resilience further solidify their potential. At its core, our strategy harmoniously melds the innate attributes of natural polyelectrolytes with contemporary 3D ink refinement techniques, offering a cost-efficient and dependable approach. The potential of this technique is vast, with promising implications for areas such as— biomimetics and soft robotics.

4. Experimental Section

Materials: Sodium hyaluronate ($M_w \approx 10^6$) was purchased from Alfa Aesar and chitosan ((50 000–190 000 Da) was purchased from Sigma. OEGMA ((oligo(ethylene glycol) methyl ether methacrylate) (M_w = 500) and EGDEMA (ethylene glycol dimethacrylate) were received from Sigma and were purified by passing through basic alumina before use. LAP (lithium phenyl-2,4,6-trimethylbenzoylphosphinate), *ortho*-nitrobenzyl chloride, and tetrabutylammonium hydroxide were also supplied by Sigma. All solvents including DMSO, acetic acid, and buffer solutions were used as received. Ultrapure MilliQ water with a resistivity of 18 MΩ cm was employed.

Characterization: ^{1}H NMR (400 MHz) spectra were recorded on a Bruker Ascend 400 NMR spectrometer at ambient temperature using D_2O as a deuterated solvent. IR spectroscopy of dried hydrogels was performed using Bruker Vertex 80 FT-IR spectrometer. The protection and deprotection of *o*-NB grafted HA were studied by UV/Vis spectroscopy using an Ocean Optics spectrometer. Moreover, SEM images of freeze-dried were taken with a Zeiss LEO 1530 microscope operating at 5 kV. Samples were sputtered with gold (thickness 5 nm) prior to measurement. For thermal studies, thermal gravimetric analysis (TGA) of freeze-dried hydrogels was carried out using a TGA 5500 (TA Instruments) at a heating rate of 10 K min^{-1} under a nitrogen atmosphere up to 600 °C, and differential scanning calorimetry of swollen hydrogel samples was conducted using a DSC Q200 (TA Instruments) ranging from −50 °C to 200 °C with a scan rate of 10 K min^{-1}.

Synthesis of HA-NB Derivative: The sodium salt of HA was converted into its acidic form by draining it through a cationic-exchange resin (Amberlite IRN-77, H^+ form), which was then neutralized by tetrabutylammonium hydroxide ($(C_4H_9)_4N^+OH^-$ to pH 7.[59] The tetrabutylammonium salt of HA was obtained after freeze-drying for 2 d. 0.1242 g of HA-TBA salt was then dissolved in dried DMSO at 40 °C. Subsequently, a solution of *ortho*-nitrobenzyl chloride (0.0343 g) in 1 mL DMSO was slowly introduced into it, and the reaction was continued at 40 °C on a magnetic stirrer for 48 h. To the resultant o-NB-grafted HA solution, a concentrated aqueous solution of NaCl (10% w/w) was added to convert it into sodium salt, which was then precipitated in acetone and filtered. Thereafter, it was washed thoroughly with acetone and dried. The obtained *o*-NB HA ester was purified extensively by dialysis against Milli-Q water for a week and then freeze-dried.

Synthesis of Photocrosslinkable P(OEGMA-co-EGDEMA) Hydrogel: A pre-gel mixture was developed by combining OEGMA and EGDEMA in a water-based solution containing LAP. This solution was subsequently exposed to UV light at a wavelength of 365 nm, leading to the formation of a hydrogel within 5 min of exposure. The successful creation of the hydrogel was validated using the inverse-vial technique, a standard method in the field.

Synthesis of PEC Hydrogel of HA-NB and CS: To synthesize a PEC, a solution of HA-NB in de-ionized water and a solution of CS in water with a few drops of 1 vol% acetic acid (AA) were prepared separately by stirring overnight. Then, a mixture was prepared by dissolving equal proportions of HA-NB and CS solutions. The mixture was stirred overnight under UV for deprotection and for the formation of PEC. The prepared solution was then poured into petri dishes and was dried in the oven at 40 °C for 48 h. Further, the obtained product was washed with water to remove any unreacted compounds. The formed PEC films were dried in a vacuum oven for a week.

Synthesis of Semi-IPN Hydrogel Containing Hyaluronic Acid or Chitosan: To synthesize semi-IPNs featuring either hyaluronic acid or chitosan, the following procedure was employed. First, HA was thoroughly dissolved in the least possible volume of water to form a solution. Subsequently, this solution was combined with a reaction mixture in water, which comprised OEGMA, EGDEMA, and LAP. On the other hand, to create a semi-IPN

containing CS, CS was dissolved in a mixture of water and 1 vol% AA to form a solution. Later, this solution was then integrated into a similar reaction mixture. These pre-gel solutions were then irradiated with UV (365 nm) for 5 min, resulting in the formation of semi-IPN hydrogels.

Synthesis of Polyelectrolyte Complex (PEC) Containing IPN Hydrogel: For obtaining PEC-incorporated IPN hydrogel, two separate solutions of HA-NB and CS were initially prepared. The HA-NB was dissolved in water, while the CS solution was prepared in a blend of water and 1% AA. These two solutions were subsequently mixed with an aqueous solution, containing OEGMA, EGDEMA and LAP. The final mixed solution exhibited a pH of approximately 4.5. To form the hydrogel, this mixture was then subjected to UV light (365 nm) for 15 min.

3D Printing Methodology: First of all, the CAD model of the print was created using Fusion 360 software and ".stl" format of the model was sliced using Miicraft Utility software. Then, the hydrogels were printed using Miicraft Hyper 80×3D printer that employs a UV source of 365 nm wavelength. The parameters set for printing included a layer thickness of 20 µm, a power ratio of 100%, UV exposure at a wavelength of 365 nm, a base curing time of 50 s and curing time of 5 s for each layer. The printing parameters (power ratio, layer thickness and curing time for each layer) were further adjusted.

Swelling Studies of Hydrogels: To determine the swelling percentage, the initial and swollen sample weights were recorded at different time intervals. The process involved taking preweighed dry samples and submerging them in deionized water. After removing the excess surface water with filter paper, the swollen samples were weighed at different time frames.

Rheological and Mechanical Testing: Disc-shaped hydrogels (25 mm diameter and 4 mm height) were prepared for the rheological measurements. The shear tests were performed at 20 °C. Rheology of as prepared hydrogels was tested at 20 °C using a shear rheometer (ARES-G2, TA-Instruments) with a Peltier (thermoelectric cooling) unit to keep the temperature constant. Further, compression tests of hydrogels (swollen in water for 15 min) were performed using a Universal Testing Machine "Inspect Table 10 kN," Hegewald & Peschke at room temperature equipped with a 1.5 kN force cell. Before the measurements, the dimensions of the samples were measured using a vernier caliper.

Supporting Information

Supporting Information is available from the Wiley Online Library or from the author.

Acknowledgements

The authors acknowledge the Ministry of Science, Research and Arts of Baden-Württemberg (MWK) for the financial support during the research. Support from the Helmholtz foundation is also greatly acknowledged.

Open access funding enabled and organized by Projekt DEAL.

Conflict of Interest

The authors declare no conflict of interest.

Data Availability Statement

The data that support the findings of this study are openly available in www.radar-service.eu at https://doi.org/10.22000/1915, reference number 1915.

Keywords

3D printing, chitosan, hyaluronic acid, interpenetrating network, polyelectrolyte complex, smart hydrogels

Received: March 26, 2024
Published online:

[1] M. Vigata, C. Meinert, D. W. Hutmacher, N. Bock, *Pharmaceutics* **2020**, *12*, 1188.
[2] S. Trombino, C. Servidio, F. Curcio, R. Cassano, *Pharmaceutics* **2019**, *11*, 407.
[3] S. Lankalapalli, V. Kolapalli, *Indian J. Pharm. Sci.* **2009**, *71*, 481.
[4] J. L. Drury, D. J. Mooney, *Biomaterials* **2003**, *24*, 4337.
[5] S. Yue, H. He, B. Li, T. Hou, *Nanomaterials* **2020**, *10*, 1511.
[6] Y. Lee, W. J. Song, J. Y. Sun, *Mater. Today Phys.* **2020**, *15*, 100258.
[7] S. Maiz-Fernandez, L. Perez-Alvarez, U. Silvan, J. L. Vilas-Vilela, S. Lanceros-Mendez, *Polymers* **2022**, *14*, 650.
[8] J. Zheng, P. Xiao, X. Le, W. Lu, P. Théato, C. Ma, B. Du, J. Zhang, Y. Huang, T. Chen, *J. Mater. Chem. C* **2018**, *6*, 1320.
[9] Q. Rong, W. Lei, M. Liu, *Chemistry* **2018**, *24*, 16930.
[10] J. Tavakoli, Y. Tang, *Polymers* **2017**, *9*, 364.
[11] J. Liu, S. Qu, Z. Suo, W. Yang, *Natl. Sci. Rev.* **2021**, *8*, nwaa254.
[12] C. Lei, Y. Guo, W. Guan, H. Lu, W. Shi, G. Yu, *Angew. Chem., Int. Ed. Engl.* **2022**, *61*, 202200271.
[13] P. Jiang, P. Lin, C. Yang, H. Qin, X. Wang, F. Zhou, *Chem. Mater.* **2020**, *32*, 9983.
[14] J. Li, C. Wu, P. K. Chu, M. Gelinsky, *Mater. Sci. Eng., R* **2020**, *140*, 100543.
[15] T. Li, F. Huang, D. Diaz-Dussan, J. Zhao, S. Srinivas, R. Narain, W. Tian, X. Hao, *Biomacromolecules* **2020**, *21*, 1254.
[16] S. E. Bakarich, R. Gorkin, R. Gately, S. Naficy, M. in het Panhuis, G. M. Spinks, *Addit. Manuf.* **2017**, *14*, 24.
[17] N. V. Arguchinskaya, E. V. Isaeva, A. A. Kisel, E. E. Beketov, T. S. Lagoda, D. S. Baranovskii, N. D. Yakovleva, G. A. Demyashkin, L. N. Komarova, S. O. Astakhina, N. E. Shubin, P. V. Shegay, S. A. Ivanov, A. D. Kaprin, *Int. J. Mol. Sci.* **2023**, *24*, 2121.
[18] S. E. Bakarich, M. I. H. Panhuis, S. Beirne, G. G. Wallace, G. M. Spinks, *J. Mater. Chem. B* **2013**, *1*, 4939.
[19] R. Zhang, N. B. Larsen, *Lab Chip* **2017**, *17*, 4273.
[20] G. Burke, D. M. Devine, I. Major, *Polymers* **2020**, *12*, 2015.
[21] Y. Wang, N. Alizadeh, M. Barde, M. L. Auad, B. S. Beckingham, *ACS Appl. Polym. Mater.* **2022**, *4*, 971.
[22] J. H. Galarraga, A. P. Dhand, B. P. Enzmann 3rd, J. A. Burdick, *Biomacromolecules* **2023**, *24*, 413.
[23] M. Taghizadeh, A. Taghizadeh, M. K. Yazdi, P. Zarrintaj, F. J. Stadler, J. D. Ramsey, S. Habibzadeh, S. Hosseini Rad, G. Naderi, M. R. Saeb, M. Mozafari, U. S. Schubert, *Green Chem.* **2022**, *24*, 62.
[24] R. Zhang, A. Liberski, F. Khan, J. J. Diaz-Mochon, M. Bradley, *Chem. Commun.* **2008**, 1317 .
[25] Q. Liu, Q. Li, S. Xu, Q. Zheng, X. Cao, *Polymers* **2018**, *10*, 664.
[26] P. R. Martinez, A. Goyanes, A. W. Basit, S. Gaisford, *Int. J. Pharm.* **2017**, *532*, 313.
[27] S. Sultan, A. P. Mathew, *Nanoscale* **2018**, *10*, 4421.
[28] V. K. Lee, G. Dai, *Ann. Biomed. Eng.* **2017**, *45*, 115.
[29] S. Waheed, J. M. Cabot, N. P. Macdonald, T. Lewis, R. M. Guijt, B. Paull, M. C. Breadmore, *Lab Chip* **2016**, *16*, 1993.
[30] A. ChimeneZolfagharian, A. Kaynak, S. Y. Khoo, A. Z. Kouzani, *3D Print. Addit. Manuf.* **2018**, *5*, 138.
[31] D. Petta, U. D'Amora, L. Ambrosio, D. W. Grijpma, D. Eglin, M. D'Este, *Biofabrication* **2020**, *12*, 032001.
[32] J. Berger, M. Reist, J. M. Mayer, O. Felt, R. Gurny, *Eur. J. Pharm. Biopharm.* **2004**, *57*, 35.
[33] S. Maiz-Fernandez, L. Perez-Alvarez, U. Silvan, J. L. Vilas-Vilela, S. Lanceros-Mendez, *Int. J. Biol. Macromol.* **2022**, *216*, 291.
[34] S. Lankalapalli, V. R. Kolapalli, *Indian J. Pharm. Sci.* **2009**, *71*, 481.

[35] S. Srivastava, M. Andreev, A. E. Levi, D. J. Goldfeld, J. Mao, W. T. Heller, V. M. Prabhu, J. J. de Pablo, M. V. Tirrell, *Nat. Commun.* **2017**, *8*, 14131.
[36] D. G. Miranda, S. M. Malmonge, D. M. Campos, N. G. Attik, B. Grosgogeat, K. Gritsch, *J. Biomed. Mater. Res., Part B* **2016**, *104*, 1691.
[37] M. Rizwan, R. Yahya, A. Hassan, M. Yar, A. D. Azzahari, V. Selvanathan, F. Sonsudin, C. N. Abouloula, *Polymers* **2017**, *9*, 137.
[38] S. Vasiliu, S. Racovita, M. Popa, L. Ochiuz, C. A. Peptu, in *Cellulose-Based Superabsorbent Hydrogels* (Eds: M. Mondal), Springer, Berlin **2019**, p. 1695.
[39] S. Li, H. Pan, Y. Wang, J. Sun, *J. Mater. Chem. A* **2020**, *8*, 3667.
[40] H. Song, Y. Sun, J. Zhu, J. Xu, C. Zhang, T. Liu, *Composites, Part B* **2021**, *217*, 108901.
[41] N. Alvarado, R. L. Abarca, C. Linares-Flores, *Int. J. Mol. Sci.* **2023**, *24*, 11535.
[42] S. Li, Q. Zhao, S. Wang, Y. Bai, K. Guo, P. Liu, X. Hu, T. Li, *Food Hydrocolloids* **2023**, *135*, 108205.
[43] A. Mora-Boza, E. Lopez-Ruiz, M. L. Lopez-Donaire, G. Jimenez, M. R. Aguilar, J. A. Marchal, J. L. Pedraz, B. Vazquez-Lasa, J. S. Roman, P. Galvez-Martin, *Polymers* **2020**, *12*, 2661.
[44] S. Suri, C. E. Schmidt, *Acta Biomater.* **2009**, *5*, 2385.
[45] Y. Liu, Y. H. Hsu, A. P. Huang, S. H. Hsu, *ACS Appl. Mater. Interfaces* **2020**, *12*, 40108.
[46] K. Bootsma, M. M. Fitzgerald, B. Free, E. Dimbath, J. Conjerti, G. Reese, D. Konkolewicz, J. A. Berberich, J. L. Sparks, *J. Mech. Behav. Biomed. Mater.* **2017**, *70*, 84.
[47] D. Li, T. Göckler, U. Schepers, S. Srivastava, *Macromolecules* **2022**, *55*, 4481.
[48] A. Bagheri, J. Jin, *ACS Appl. Polym. Mater.* **2019**, *1*, 593.
[49] H. Zhao, E. S. Sterner, E. B. Coughlin, P. Theato, *Macromolecules* **2012**, *45*, 1723.
[50] F. Horkay, *Gels* **2021**, *7*, 102.
[51] S. J. Kim, K. J. Lee, S. I. Kim, *J. Appl. Polym. Sci.* **2004**, *93*, 1097.
[52] M. Gierszewska, J. Ostrowska-Czubenko, E. Chrzanowska, *Eur. Polym. J.* **2018**, *101*, 282.
[53] R. Foudazi, R. Zowada, I. Manas-Zloczower, D. L. Feke, *Langmuir* **2023**, *39*, 2092.
[54] G. S. Sailaja, P. Ramesh, T. V. Kumary, H. K. Varma, *Acta Biomater.* **2006**, *2*, 651.
[55] V. M. Gun'ko, I. N. Savina, S. V. Mikhalovsky, *Gels* **2017**, *3*, 37.
[56] C. Lin, I. Gitsov, *Macromolecules* **2010**, *43*, 3256.
[57] R. Kocen, M. Gasik, A. Gantar, S. Novak, *Biomed. Mater.* **2017**, *12*, 025004.
[58] S. Maiz-Fernandez, N. Barroso, L. Perez-Alvarez, U. Silvan, J. L. Vilas-Vilela, S. Lanceros-Mendez, *Int. J. Biol. Macromol.* **2021**, *188*, 820.
[59] C. Pozos Vázquez, T. Boudou, V. Dulong, C. Nicolas, C. Picart, K. Glinel, *Langmuir* **2009**, *25*, 3556.